The influence of plastic flow localization on the surface morphology of aluminum alloy specimens subjected to complex loading

Evgeniia A. Chechulina
Ural Research Institute of Composite Materials, Perm, Russia
zhenya-chechulina@yandex.ru, https://orcid.org/0000-0003-4834-7911

Vladimir A. Oborin
Institute of Continuous Media Mechanics, Perm, Russia
oborin@icmm.ru, http://orcid.org/0000-0003-2836-2073

Dmitriy S. Gribov
Perm National Research Polytechnic University, Perm, Russia
gribovds@pstu.ru, http://orcid.org/0000-0001-6838-3122

Citation: Chechulina E.A., Gribov D.S., Oborin V.A., The influence of plastic flow localization on the surface morphology of aluminum alloy specimens subjected to complex loading, Fracture and Structural Integrity, 71 (2024) 223-238.

Received: 15.09.2024
Accepted: 13.11.2024
Published: 19.11.2024
Issue: 01.2025

KEYWORDS. Portevin–Le Chatelier effect, Al-Mg alloys, Complex (nonproportional) loading, Surface morphology, Wavelet analysis, Profilometric analysis.

INTRODUCTION

An important characteristic determining the quality of products obtained by plastic deformation methods, especially in finishing operations, is the roughness of their surface. It is known that in certain ranges of temperatures and deformation rates, the Portevin-Le Chatelier effect (and further in the text – PLC) occurs in almost all alloys,

causing localization of deformation, which manifests itself in the appearance of clearly distinguishable stripes on the surface [1, 2]. As a result, the initially smooth surface becomes rough, which degrades the products performance and can cause their premature corrosion and sudden destruction [3 - 7].

Taking into account the widespread use of Al-Mg alloys as structural materials for the automotive industry, in the aerospace industry, where there are tight constraints on roughness tolerances for stampings, the issue of establishing areas in the space of influencing characteristics (strain rates and temperatures) in which the Portevin-Le Chatelier effect is realized is relevant in order to determine the technological process modes in which this effect does not occur [8].

To study the PLC effect in metallic materials, particularly in Al-Mg alloys, simple types of loading are most often used, for example, uniaxial loading on flat specimens. Moreover, the great importance are optical methods and means of non-destructive testing, which allow non-contact registration of spatial inhomogeneity of plastic flow, such us, the Digital Image Correlation method (DIC) [9, 10], which allows fixing the evolution of deformations and displacement; digital statistical speckle interferometry [10], which makes it possible to register foci of deformity localization "in situ"; optical and electron microscopy [11]; acoustic emission [12].

The methodology and results of experiments on uniaxial loading of flat specimens' different thicknesses (0.5, 1.0, 1.5 mm with a width of 4 mm) made of aluminum alloy AA5754 are presented in [13]. Digital image correlation method was used for the measurements.

The article [10] considers an experimental, theoretical and numerical study of the effects of strain rate on the PLC characteristics of the aluminium–magnesium alloy (AA5083-H116) specimens. Digital image correlation and digital infrared thermography were used to determine the propagation velocity and width of the shear bands. The experiment was carried out on a kinematic – type machine at deformation rates of 3.33×10^{-3} and 10^{-1} s^{-1}.

The spatiotemporal aspects of the Portevin-Le Chatelier instability, using infrared thermography, in an Al-4.5%Mg alloy loaded at room temperature in simple tension are investigated in [14].

Experimental data and physical mechanism that cause the occurrence of discontinuous plasticity during deformation at room temperature at different deformation rates of aluminum-magnesium alloy specimens (Al-2.6%Mg; Al-3%Mg; 4.8%Mg, etc.) discussed in [12]. The acoustic emission method was used for the study.

The aim of the work is to study the influence of effect of plastic flow localization on the surface morphology of Al-6% Mg alloy specimens subjected to complex loading. The paper presents the results of a study of the deformation relief of the surfaces of thin-walled tubular specimens of aluminum-magnesium alloy (Al-6% Mg) subjected to complex loading before and after testing using a New View 5000 optical three-dimensional profilometer-interferometer. The surface of the specimens was studied at different scale levels depending on the deformation program.

The specimens were loaded according to the following programs:

simple loading: a) uniaxial loading, b) shear, c) proportional loading by tension – shear;

complex (nonproportional) loading: d) shear → tension, e) proportional loading → tension.

The results obtained according to the simple loading programs were published earlier [15], in this paper the results obtained under complex loading are presented.

The data of scanning the surface profiles were obtained only in the initial (reference) configuration and at the moment of completion of deformation; studies of the surface profile at intermediate moments were not contemplated. Diagrams of dependency of the height profile on the coordinate along two selected directions (meridional and axial cross-section of the specimen) of the selected sections of the specimen surfaces were obtained.

EXPERIMENTAL METHODS AND RESULTS

In real technological processes, the material experiences complex loading at the macro level; despite this, in order to study PLC, in the overwhelming majority of studies experiments are carried out on uniaxial loading on solid flat or cylindrical specimens, therefore, to study the influence of the nature of surface layers deformation on the quality of parts (articles) surface, cylindrical tubular specimens were chosen, for which it is possible to conduct complex loading tests.

Mechanical testing

The specimens for mechanical testing (Fig. 1) were made from a tubular workpiece (outer diameter Ø28 mm, wall thickness 5 mm) of structural aluminum-magnesium alloy Al-6%Mg. The specimens were annealed in a muffle furnace in air at 400°C for 3 hours and cooled in the furnace to room temperature. The surface roughness after manufacturing and annealed was Ra 0.05 mm. The cut out specimens were mechanically processed using sandpapers with a gradual decrease in abrasive grain

from 600 to 2500 and subsequent polishing with GOI (chromium oxide) pastes to obtain a mirror-like working surface. The surface roughness after polishing was Ra 0.2 μm.
The chemical composition of the alloy in mass fractions is presented in Tab. 1.

Al	Mg	Mn	Fe	Si	Zn	Ti	Cu	Be
92.55	6.12	0.84	0.27	0.17	0.005	0.039	0.001	0.005

Table 1: The chemical composition of the used alloy.

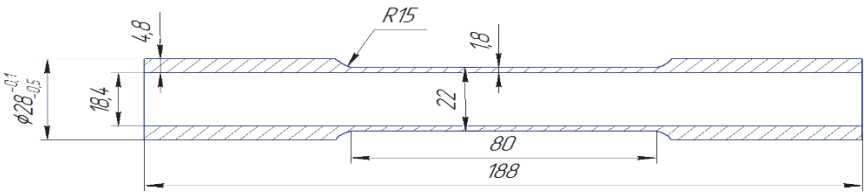

Figure 1: Sketch of a thin-walled tubular test specimen.

Mechanical testing was implemented on the Instron 8850 two-axis servo-hydraulic testing system at room temperature of 21 °C. A more detailed description of the methodology for experimental studying the mechanisms of initiation and propagation of deformation bands of localized plastic flow, determining the boundaries of discontinuous plastic deformation of the Al-6% Mg alloy under complex loading conditions are presented in [16].

Registration of inhomogeneous displacement and strain fields was carried out by using the Vic-3D digital image correlation measurement system. The shooting of specimens was realized with a set of high-resolution cameras (Prosilica, 16 Mp), the shooting speed was 3 frames per second, the dimension of the subset was 29x29 pixels, the subset distance was 3 pixels. The criterion of the normalized sum of squared differences was used as the least sensitive to changes in illumination (brightness) of the sample during deformation and providing the best combination of time costs and accuracy of results.
The trajectories changed at accumulated strains exceeding the critical strain for the manifestation of the PLC effect (ε_{cr}). The following complex loading programs were implemented: a) "shear (γ) → tension (ε)" at a strain rate of $\dot{\gamma} = 9.35 \cdot 10^{-4}\, 1/s$ and $\dot{\varepsilon} = 5.389 \cdot 10^{-4}\, 1/s$, b) "proportional loading (tension + shear) → tension" at a strain rate of: ($\dot{\varepsilon} = 5.389 \cdot 10^{-4}\, 1/s$ + $\dot{\gamma} = 0.675 \cdot 10^{-4}\, 1/s$) → $\dot{\varepsilon} = 5.389 \cdot 10^{-4}\, 1/s$. Fig. 2 shows the complex loading trajectories in the coordinates "axial strain ε – shear strain γ" for specimens No. 1 and 2. Fig. 3 show the resulting "equivalent stress–accumulated equivalent strain" diagram for the corresponding trajectories "shear (γ) → tension (ε)".

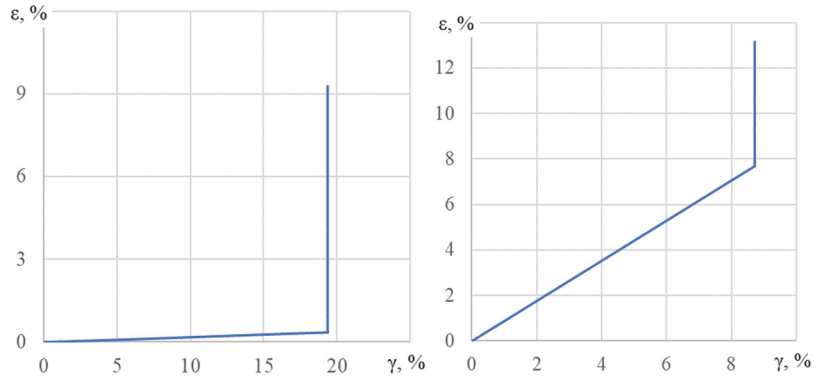

(*a*) (*b*)

Figure 2: Deformation trajectories of specimens No. 1 (*a*), 2 (*b*) (specimens No. 8, 9, respectively, in [17]).

In tests for simple loading, the values of critical shear strains for shear and critical strains for uniaxial loading, as well as the values of critical equivalent strain under proportional loading (shear combined with tension) were determined [18]. The value of critical strain, which corresponds to the moment of the onset of discontinuous yielding and the formation of

deformation bands of PLC effect, was 5.59% in the uniaxial tension test; in tests for proportional loading, the critical equivalent strain was 5.43%. Based on the video system data, the critical value of shear strain under shear loading γ_{cr} was determined to be 1.69%.

Three main types of the PLC effect manifestation are distinguished: 1) type A - characterized by repeated stress "jumps" (hereinafter jumps) of small amplitude and average frequency of equivalent stress in relation to the smoothed curve; 2) type B – deformation bands appear and disappear in an oscillating or intermittent mode with a high frequency, propagating along the specimen (stop-and-go) with a greater amplitude than type A jumps; 3) type C – bands appear (and disappear) randomly along the length of the specimen with low frequency and high amplitude. In field experiments, various combinations of these three types are observed.

Loading along the trajectory "shear → tension"

The test results for loading along the trajectory "shear → tension" (Fig. 2(*a*)) for specimen No. 1 are shown in Fig. 3. The change in the loading mode was made after reaching the critical deformation of the manifestation of the PLC effect for shear. The moment of changing the loading trajectory is highlighted by a dotted line.

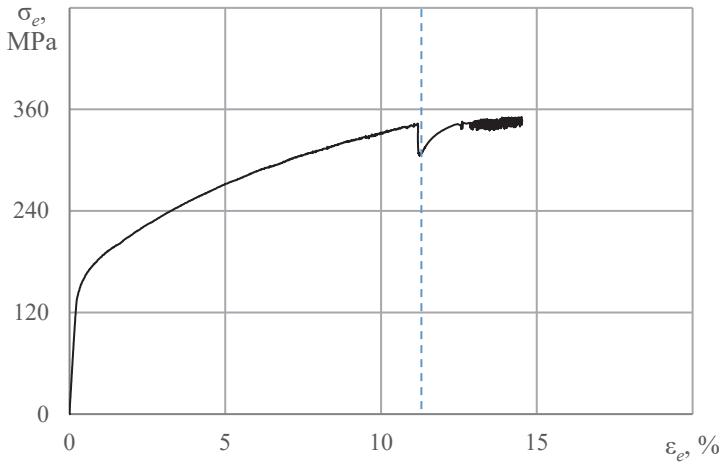

Figure 3: Diagram "equivalent stress – of accumulated equivalent strains" of specimen No. 1 under shear followed by tension.

The loading diagram of specimen No. 1 contains stress jumps of small amplitude, and the localization of plastic deformation is weakly expressed. To assess the degree of nonuniformity (heterogeneity) of plastic deformation, the fields of local shear and longitudinal deformation rates are presented. The picture of the fields illustrates the spread of values of the local shear deformation rate (Fig. 4).

When loading the specimen with shear (before the fracture of the deformation trajectory, Fig. 2(*a*), A-type bands are observed (Fig. 3). After the transition from shear to uniaxial tension, the effect of discontinuous yielding is not observed for some time, therefore, the change in trajectory does not lead to the simultaneous occurrence of spatiotemporal inhomogeneity of the stress-strain state. With further stretching of the specimen, bands of localized plastic flow are again recorded on the material surface, characteristic of the implementation of PLC effect in the type B mode.

Plastic deformation at the initial stage (formation of deformation bands) occurs along the planes of action of maximum tangential stresses. Consequently, the shear bands during shear are oriented perpendicular to the axis of specimen No. 1 (Fig. 4(*a*), 4(*b*)), after changing the loading trajectory from shear to tension, the pattern of distribution of bands in specimen No. 1 changes (Fig. 4(*c*), 4(*d*)).

Loading along the trajectory "proportional loading → extension"

The test results for loading along the trajectory "proportional loading → extension" for specimen No. 2 are shown in Fig. 5. The loading trajectory was changed over after the onset of the PLC effect for proportional loading. The moment of changing the loading trajectory is highlighted by a dotted line.

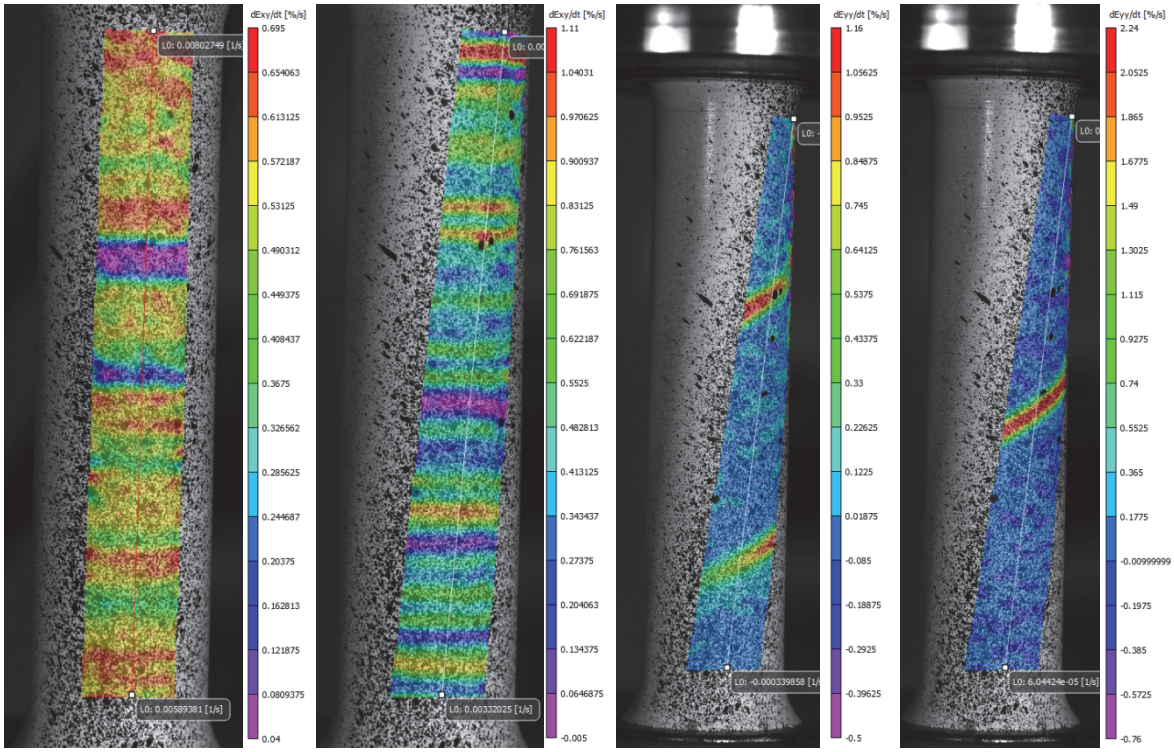

(*a*) (*b*) (*c*) (*d*)

Figure 4: Fields of shear deformation rates (*a* – 7 sec, *b* – 17 sec) and longitudinal deformation rates (*c* – 229 sec, *d* – 238 sec), which correspond to the values of the of accumulated equivalent strain (*a* – 4.21%, *b* – 10.11%, *c* – 23.29%, *d* – 23.83%) for a specimen subjected to shear followed by tension.

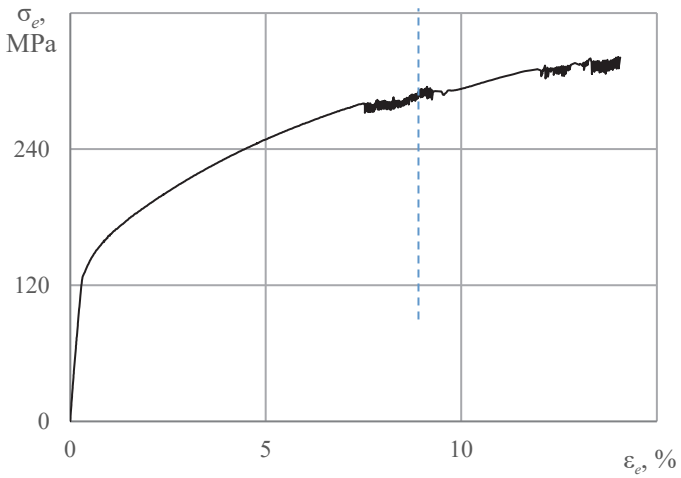

Figure 5: Deformation diagram "equivalent stress– accumulated equivalent strain" under proportional biaxial loading followed by stretching of specimen No. 2.

As an example, the fields of shear strain rates and longitudinal strain rates are given for both loading trajectories of specimen No. 2: under proportional loading (Fig. 6 (*a*, *b*)) and uniaxial tension (Fig. 7 (*c*, *d*)).

The deformation diagram for loading followed by stretching of specimen No. 2 (Fig. 5) shows stress drops of small amplitude before changing of the loading trajectory. The kinetics of band formation in this case corresponds to discontinuous yield of type B. After the transition from proportional biaxial loading to uniaxial tension, the diagram shows discontinuous yield, characteristic of the mixed type (B+C).

The distribution pattern of deformation bands in specimen No. 2 under proportional (before the trajectory change) and uniaxial tension (after the trajectory change) is similar. However, different values of the angle between the PLC bands and the loading axis are observed in the case of proportional and uniaxial loading.

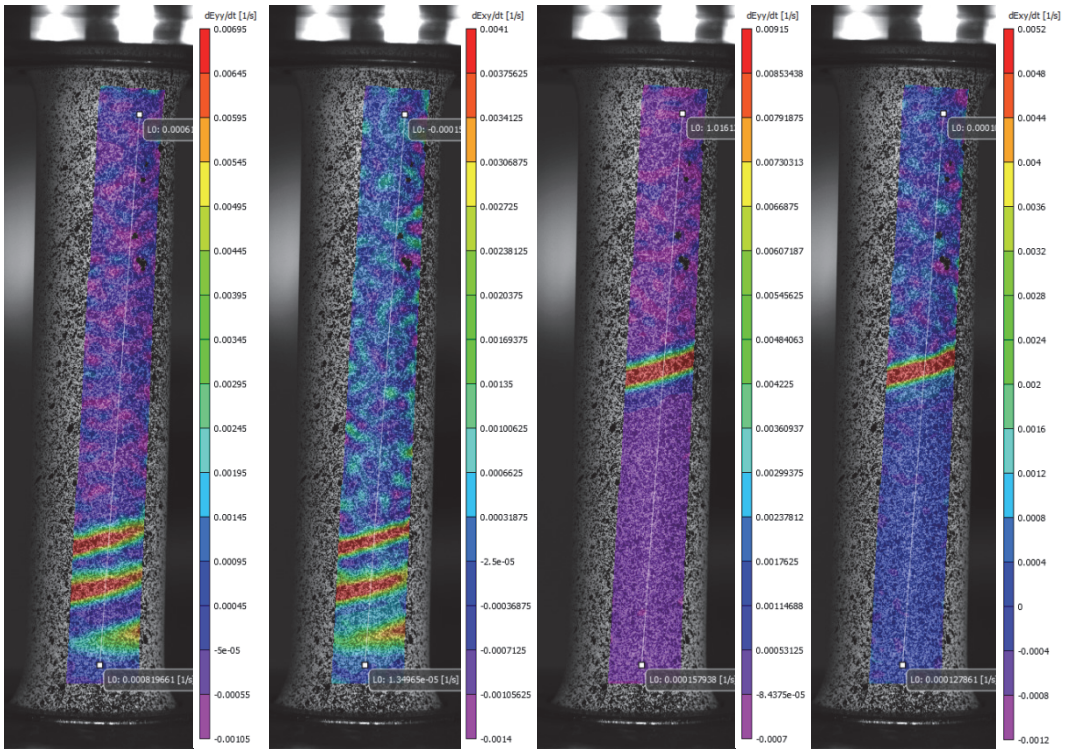

(*a*) (*b*) (*c*) (*d*)

Figure 6: Fields of longitudinal (*a* – 109 sec, *c* – 112 sec) and shear (*b* – 109 sec, *d* – 112 sec) deformation rates, which correspond to the values of the accumulated equivalent strain (*a,b* – 8.59%, *c*, *d* – 8.78%) for a specimen subjected to proportional biaxial loading.

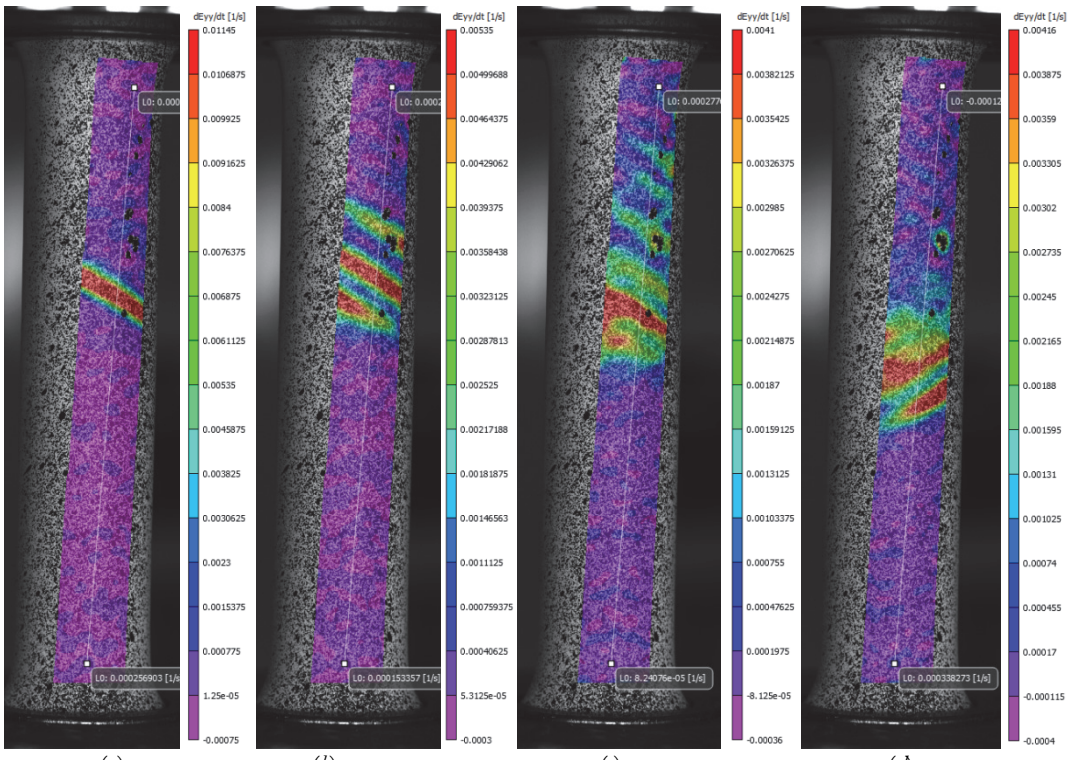

(*a*) (*b*) (*c*) (*d*)

Figure 7: Fields of longitudinal strain rates (*a* – 214 sec, *b* – 216 sec, *c* – 218 sec, *d* – 220 sec), which correspond to the values of the accumulated equivalent strain (*a* – 15.01%, *b* – 15.11%%, *c* – 15.22%%, *d* – 15.32%) for a specimen subjected to uniaxial tension.

Studies using an optical profilometr-interferometr

The localization of plastic flow was studied by the structural analysis of the morphology of the surface using the optical interferometer-profilometer New View-5010 (at x1000 magnification). Microstructural analysis of deformed and undeformed specimens consisted of calculating the scale invariant (Hurst exponent) and the spatial scale of the region in which correlated behavior of microshears is observed according to the interferometer-profilometer data in the areas of plastic deformation localization, namely in three regions on the surface of the specimen: in the central region and near the grippers (Fig. 8). Zone 1 is located near the end of the specimen, which was clamped in the upper collet gripper, zone 2 - in the central part of the specimen, zone 3 - near the second gripper. To indicate the measurement area, local coordinates were set in the tangent plane to the cylindrical surface, one axis is located parallel to the sample axis, the second is orthogonal to it, and the third axis is orthogonal to the tangent plane (Fig. 8). The specimen sections along the meridional direction are highlighted in black in Fig. 8, and in the axial section of the specimen - in red.

Figure 8: Measurement area on the surface of a tubular specimen.

When using a contact profilometer, the maximum difference in height is determined based on which area gets into the analysis zone (on the scanning line), the minimum value will correspond to the "troughs", and the maximum - to the "peaks" (heights).

Using a contact profilometer, a 3D map of the surface was created (Fig. 9(*b*)), then the results of surface roughness measurements at the moment of completion of deformation (Fig. 9(*a*)) were analyzed using fractal analysis methods.

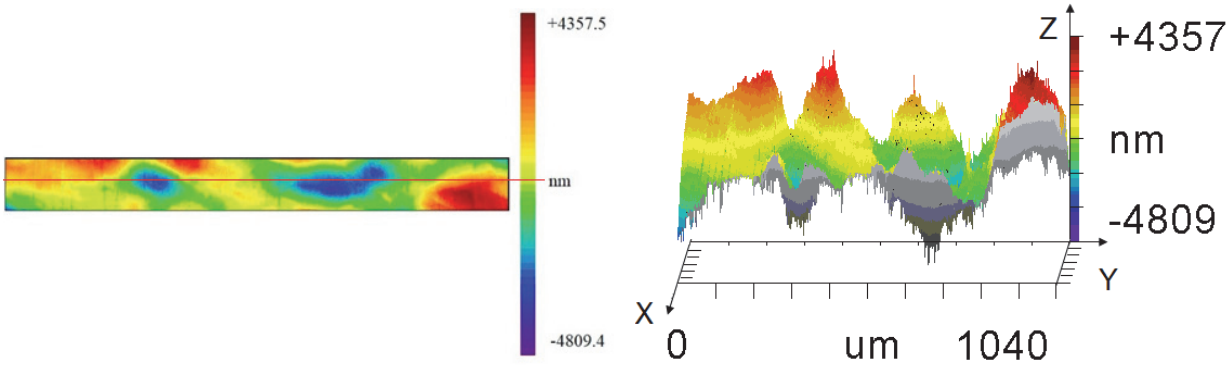

(*a*) (*b*)

Figure 9: Surface height map indicating the location of profile selection (*a*) and three-dimensional projection of the surface of specimen No. 2 after deformation (*b*).

The Hurst exponent is estimated by fitting the power law r^H to the experimental data on the measurement of the surface roughness of the specimen:

$$(x, y, z) \rightarrow (bx, by, b^H z) \tag{1}$$

where z is the height, x and y are the coordinates in the plane perpendicular to z-direction, H is the roughness index or Hurst exponent.

Eqn. (1) generally implies that the height $K(r)$ at a point $r = \sqrt{x^2 + y^2}$ is given by the function:

$$K(r) = \left\langle (z(r_0 + r) - z(r_0))^2 \right\rangle_{r_0}^{1/2} \propto r^H \quad (2)$$

where r is the length of the segment on which the difference in heights is located; $K(r)$ is the averaged difference in values (the number of interferometer step points) of the surface relief heights $z(r_0+r)$ and $z(r_0)$ on a window of size r, $z(r_0)$ is the height at the initial point r_0; $z(r_0+r)$ is the height at the point shifted by r. The $\propto$ sign denotes asymptotic equality (the notation was introduced in articles [19; 20] on the Hurst exponent definition). To determine the length, the number of points per interferometer step is multiplied by the set magnification value.

Within each "window" measuring 105x1040 μm (in the region of maximum shear deformations), 13 one-dimensional profiles were analyzed, with a vertical resolution of ~0.1 nm and a horizontal resolution of ~0.25 μm. The $K(r)$ function was calculated from one-dimensional profiles of the surface relief in the region of maximum shear deformations (Fig. 10(*a*) – 11(*a*)).

It is possible to determine the Hurst exponent by plotting the $\log_2 K(r)$ graph as a function of $\log_2(r)$. The slope angle is determined from the function graph by linear approximation using the least squares method of the longest straight section; a straight line is drawn with a reliability of R^2~0.99. The tangent of this angle is the Hurst exponent. The shape of the curve changes with a change in the Hurst exponent; as it increases, the original profile becomes less noisy. As the Hurst exponent approaches 1, the original profile approaches a straight line.

It has been theoretically proven that for a random process (Brownian motion) the Hurst exponent H = 0.5. Based on extensive empirical material, it has been shown [21] that for many natural processes and phenomena the Hurst exponent lies in the range H = 0.72 – 0.74, which is true for processes that have a trend component (the presence of memory and the preservation of an existing trend). Anti-persistent systems that exhibit cyclicity (after growth there is a decline) yield values of the exponent H< 0.5.

In the works of M. Zaiser and E. Bouchaud [19, 20], for the quantitative characteristic of self-similar surface structures (in our case, after deformation, the Hurst exponent is greater than 0.5), formed during the deformation and destruction of loaded solids, a method was proposed based on the concept of scale invariance of the deformed surface, allowing the application of fractal theory for its description and quantitative assessment. The main method for studying the fractal structure of the surface is the measurement of the fractal dimension and the Hurst exponent, invariant with respect to scale transformation. Fractal dimension is a coefficient describing fractal structures or sets based on a quantitative assessment of their complexity, as a coefficient of change in a part with a change in scale.

The Hurst exponent H takes on a value from 0 to 1 and is related to the fractal dimension D ("window dimension") of the entire structure by the relation:

$$D = D_T - H \quad (3)$$

where D is the fractal dimension; D_T is the Euclidean (topological) dimension of the object (2 for the profile and 3 for the surface); H is the Hurst exponent. Research shows that the smaller H, the rougher the surface, and therefore the greater the fractal dimension. Thus, the value of the fractal dimension can be used as a characteristic of surface roughness, since this value adequately reflects changes in the profile structure and is associated with the degree of its irregularity.

The representation of the $K(r)$ function in logarithmic coordinates in accordance with relation (1) allows to estimate the Hurst exponent – H as a spatial invariant determined by the constancy of the slope of the $\log_2 K(r)$ dependence on $\log_2(r)$ in the range of scales (l_{sc}, L_{pz}), Fig. 9(*b*). The value of the lower boundary of the linear section of the $K(r)$ function was taken as the value of the critical scale l_{sc} – the minimum spatial scale in the vicinity of the deformation zone, on which scale-invariant patterns of the relief begin to appear, the value of the upper boundary L_{pz} was taken as the value of the scale associated with the maximum region of correlated behavior of shear bands generated by collective movements of dislocations along closely spaced slip systems (Fig. 10(*b*)). The values of the lower l_{sc} and upper L_{pz} scales are necessary to determine the spatial scales that cause the correlated behavior of defects (dislocation arrays) in the region of deformation localization.

The Hurst exponent was determined by the boundaries of the longest straight section on the $\log_2 K(r)$ graph as a function of $\log_2(r)$ a straight line is drawn with confidence R^2~0.99. Since the graphs in Fig. 10 and 11 are constructed in logarithmic coordinates, the experimental points are located very close to the lower boundary and visually it seems that the lower boundary can be shifted to the right, but for mathematical accuracy we chose the same confidence R^2~0.99 for all graphs. The graphs in Fig. 10 and 11 show only typical data for only two profiles, and 13 profiles were measured for each site and averaging was performed.

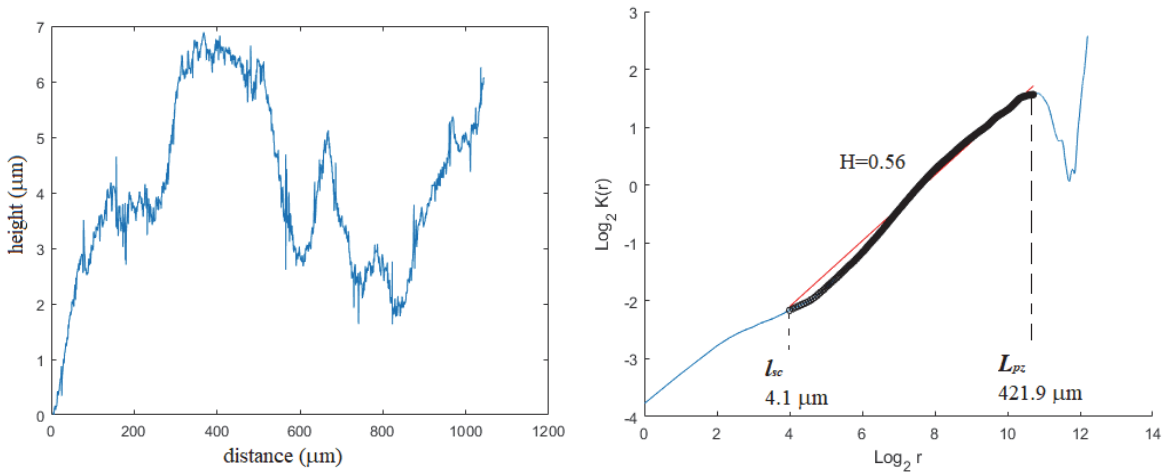

(*a*) (*b*)

Figure 10: Characteristic one-dimensional profile after deformation (*a*); type of dependence of $\log_2 K(r)$ on $\log_2(r)$ for the surface of specimen No. 1 after deformation (*b*).

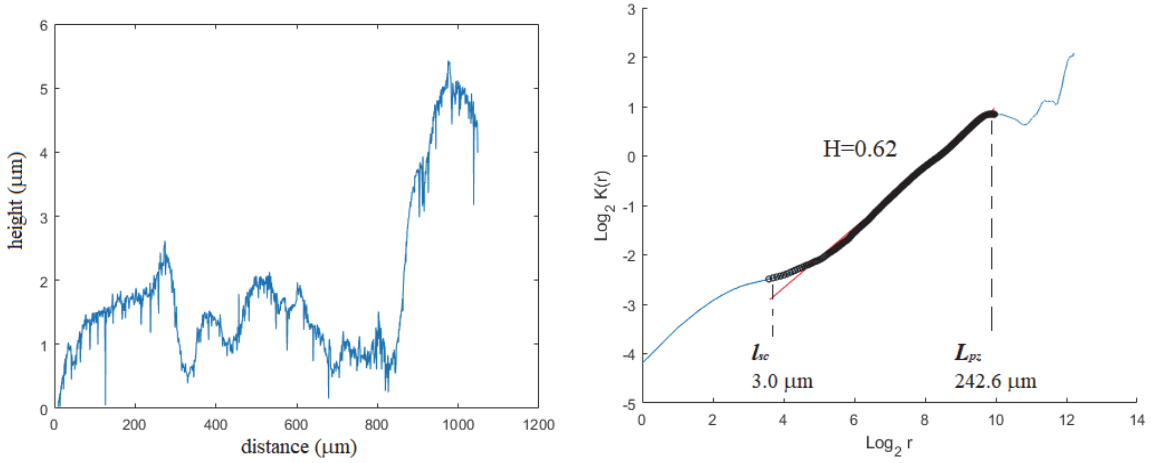

(*a*) (*b*)

Figure 11: Characteristic one-dimensional profile after deformation (*a*); type of dependence of $\log_2 K(r)$ on $\log_2(r)$ for the surface of specimen No. 2 after deformation (*b*).

Tab. 2 shows the values of roughness after deformation, the Hurst exponent and the corresponding spatial scales for specimens subjected to complex loading, in the initial and deformed state. The surface roughness value of all polished specimens in the reference configuration (before conducting experiments on simple and complex loading) was Ra=0.2 μm. Tab. 3 shows similar results for simple loading (uniaxial tension and shear loading) and proportional loading, considered in the previously published article of the authors [15].

Comparative analysis of scale-invariant characteristics of specimens of Al-6%Mg alloy in the initial state and deformed by complex loading allowed to establish a significant increase in the Hurst exponent to H~0.56-0.62 in a wide range of spatial scales of 3.0-421.9 μm, in contrast to undeformed specimens (H~0.18-0.32 in the range of spatial scales of 0.6-34.1 μm). On all specimens before deformation, the Hurst exponent was approximately equal to white noise, and after deformation, correlations in the relief appeared. Considering that the Hurst exponent is estimated by measuring the roughness of the specimen surface, there was an increase in the roughness of the specimen due to the occurrence and passage of slip bands on the surface of the specimen.

Specimen No.	Before deformation			After deformation			
	H	l_{sc} μm	L_{pz} μm	H	l_{sc} μm	L_{pz} μm	Ra μm
1	0.18±0.02	0.6±01	34.1±12.8	0.56±0.01	4.1±2.6	421.9±17.1	0.28±0.02
2	0.32±0.02	0.6±0.1	3.3±0.2	0.62±0.02	3.0±1.1	242.6±20.1	0.24±0.02

Table 2: Values of the Hurst exponent and spatial scales for complex loading.

Loading type	Before deformation			After deformation			
	H	l_{sc} μm	L_{pz} μm	H	l_{sc} μm	L_{pz} μm	Ra μm
Uniaxial tension	0.21±0.01	0.5±0.1	2.9±0.1	0.59±0.01	1.7±0.5	169.9±10.8	0.50±0.03
Shear	0.30±0.03	1.6±0.5	188.8±44.2	0.49±0.03	14.3±5.5	136.1±10.1	0.29±0.02
Proportional loading	0.44±0.01	2.9±0.7	176.9±7.8	0.64±0.03	8.4±4.6	162.1±15.2	0.54±0.05

Table 3: Values of the Hurst exponent and spatial scales for simple loading.

When comparing the results obtained under simple and complex loading, a significant increase (two times as much for specimen No. 1) in the correlation of structural elements at large distances is observed, which can lead to the formation of extensive areas of increased roughness.

In this case, a slight increase in the value of the Hurst exponent is observed; with simple loading, the value of the exponent reaches H~0.49-0.59, for complex loading H~0.56-0.64. In this case, the Hurst exponent reaches the highest value of H~0.64 with proportional loading.

Due to the fact that the patterns of shear bands on the specimen obtained using DIC at the final stage of deformation are periodically repeated, the authors of the work attempted to relate the locations of roughness obtained on the profilometer to the locations of shear bands on the specimens (Fig. 4, 6, 7). For this purpose, one-dimensional sections of the surface relief along the tensile axis were analyzed in three areas: in the area of the left gripper, in the central area, in the area of the right gripper. On both specimens No. 1, 2, waves running along the specimen were recorded in the central part, which are localized deformation bands. Considering that the patterns of localized deformation bands on the specimens are periodically repeated, further in the text one-dimensional surface profiles are described for different programs of complex loading precisely in the central part of the specimens.

The surface profile data was obtained in the initial (reference configuration) and after the completion of deformation. The graphs of the height profile dependencies on the coordinate were obtained as the value of the one-dimensional profile data along the selected direction in the meridional and axial sections of the specimen.

Figs. 12-15 show the obtained one-dimensional section profiles. For the meridional sections, an assessment of the need to exclude the main surface shape (cylindricity) was taken. The length of the line along which the measurements were made, determined in the scanning area along the circular section is 0.5 mm. The calculated value of the chord length based on the same central angle is 0.50011 mm, as a result of which the curvature of the surface in the meridional direction can be neglected in the measured section and approximated by a section of the plane.

The surface roughness of polished specimens before testing was Ra=0.2 μm. After mechanical testing, the surface roughness of the specimens increased (see Tabs. 2-3).

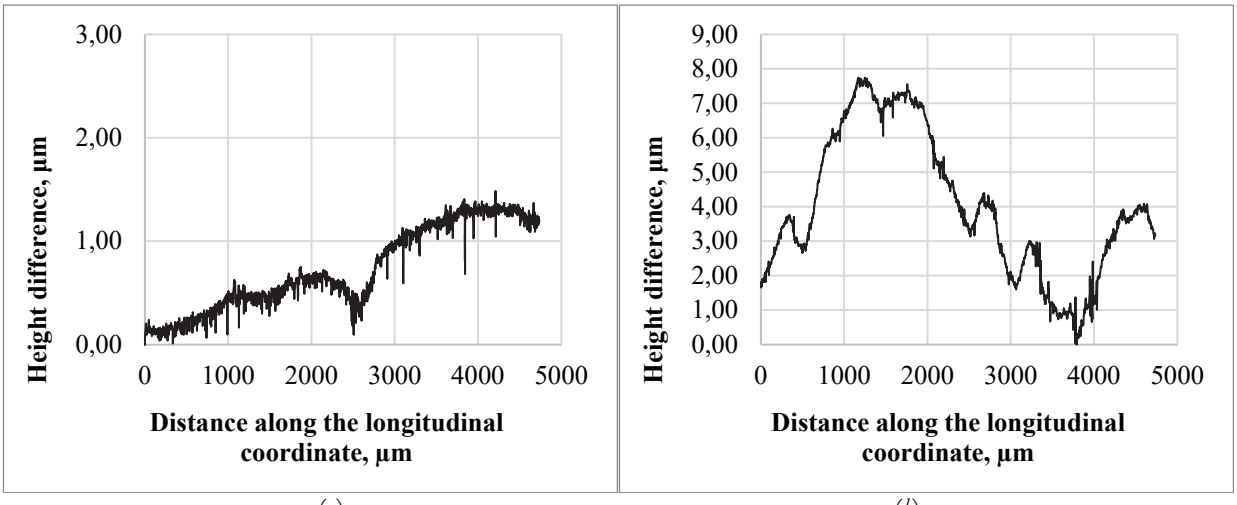

(*a*) (*b*)

Figure 12: Characteristic one-dimensional profile before deformation (*a*); after deformation (*b*) for the surface of specimen No. 1 in its axial section.

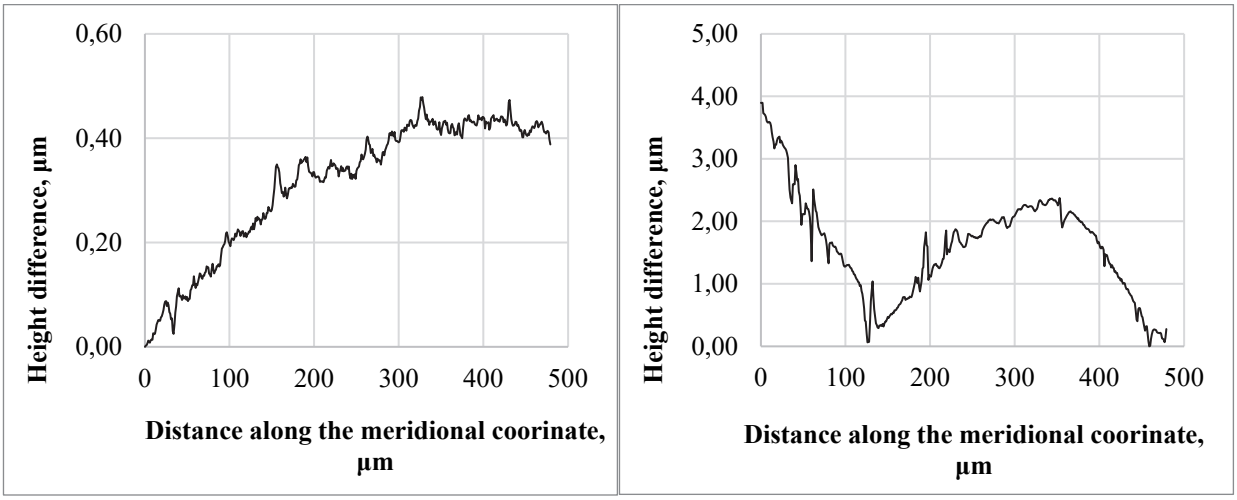

(*a*) (*b*)

Figure 13: Characteristic one-dimensional profile before deformation (*a*); after deformation (*b*) for the surface of specimen No. 1 in its meridional direction.

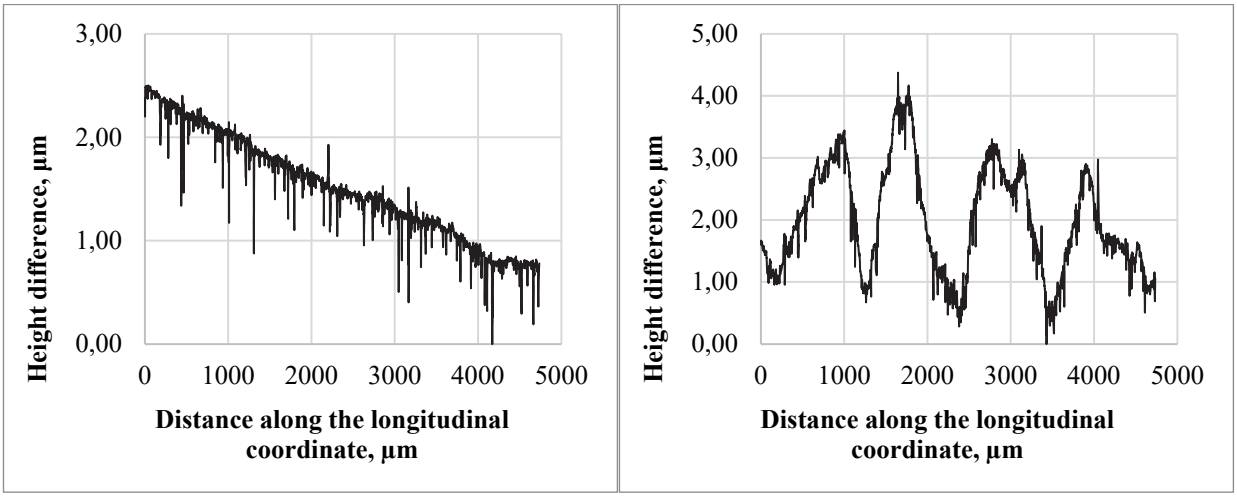

(*a*) (*b*)

Figure 14: Characteristic one-dimensional profile before deformation (*a*); after deformation (*b*) for the surface of specimen No. 2 in its axial section.

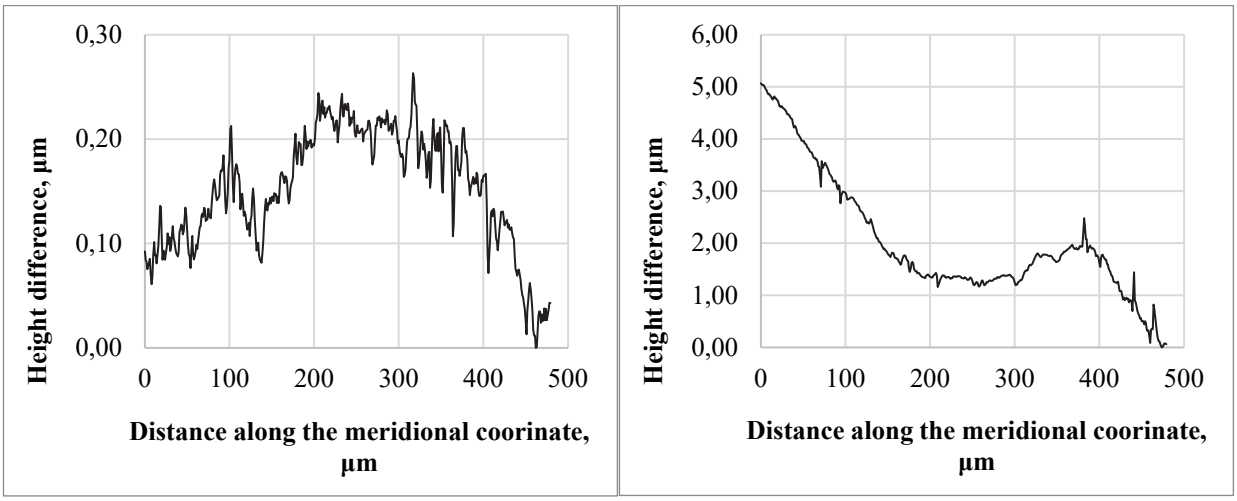

(*a*) (*b*)

Figure 15: Characteristic one-dimensional profile before deformation (*a*); after deformation (*b*) for the surface of specimen No. 2 in its meridional direction.

In this case, the highest roughness Ra=0.5 μm is observed under uniaxial tension and proportional loading, in contrast to shear loading and complex loading (shear → tension; proportional loading → tension) for which the roughness did not exceed Ra=0.29 μm.

The roughness obtained in the reference configuration is the result of insufficiently thorough polishing of the specimen. After mechanical testing, the profile patterns of the side surfaces change qualitatively, small roughness is "absorbed" in the surface profiles of the loaded specimens. The profile is smoothed, but instead of small roughness, a wave grows, running along the specimen. It is possible that small amplitude jumps are stretched together with the outer layers of the specimen material.

Note: On the meridional one-dimensional profiles, the surface of the specimen seems cylindrical, despite the fact that during the assessment it was accepted to neglect the curvature of the surface in the meridional direction on the measured section and to approximate it with a section of the plane; this feature is possibly associated with the fact that the tip of the profilometer indenter slides during the determination of the profile roughness along the real meridional direction, which is a section of a circle.

In order to relate the location of the roughness obtained with the profilometer to the locations of the shear bands on the specimen, scalograms of the surface profile of the specimens and scalograms of the graphs of the accumulated radial deformations of the specimens were constructed using wavelet analysis. The results of the comparison of scalograms for specimen No. 2 are presented in Fig. 18-19.

Analysis of profilograms using wavelet analysis

The obtained optical images of macro- and microrelief in the form of one-dimensional profiles (Fig. 12-15) of the sections of the surface of aluminum alloy specimens before and after complex loading were processed using wavelet analysis for the results of measurements along the meridional direction and the direction parallel to the specimen axis. The wavelet transform [22; 23] is widely used for signal analysis, in particular, for filtering, compressing information, etc. On wavelet transform scalograms, the values reflect the level of contribution of a component with a certain "frequency" and scale to the overall signal. The term "frequency" is used by analogy, since wavelet analysis is most often used for time series analysis. Instead of physical time, a non-decreasing parameter is used here – the accumulated equivalent deformation (as is often done in the theory of plasticity). The brighter the color of the area on the scalogram, the greater its contribution to the overall signal.

Figs. 16*a*–16*b* present the results of the analysis of profilograms in the tensile axis direction and in the meridional direction under complex loading of specimen No. 2 "proportional loading → stretching" during deformation of specimens in the range of manifestation of the PLC effect. To study the original signal using a continuous wavelet transform, a family of complex Morlet wavelets was used [24], which allows for good localization of signal "frequencies" that appear only in part of it (as the effect of discontinuous plasticity also appears).

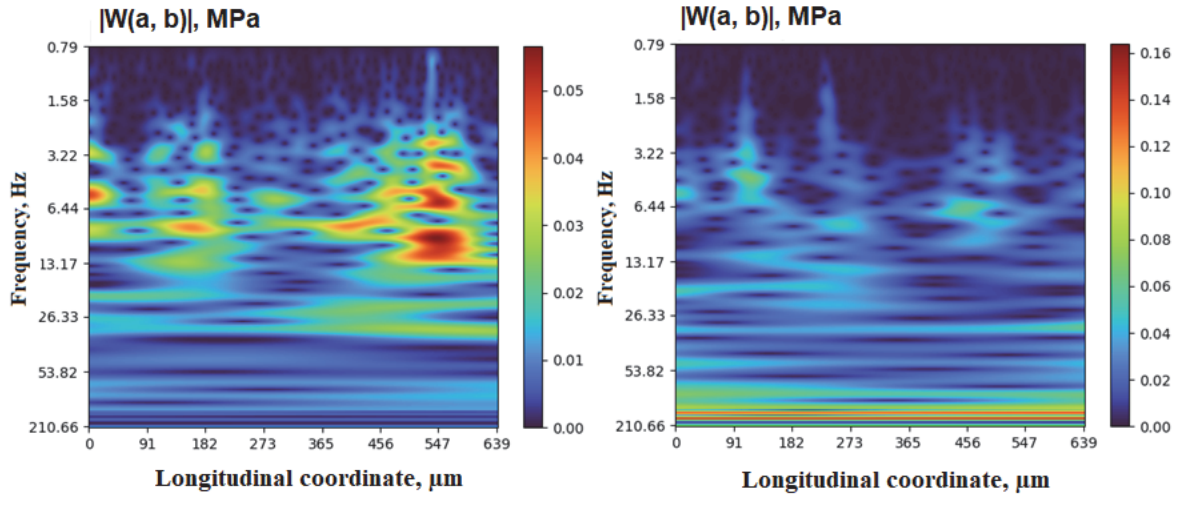

(*a*) (*b*)

Figure 16: Scalogram of the surface profile of specimen No. 2 along the loading axis: before deformation(*a*); after deformation (*b*).

The scalogram shown in Fig. 16 corresponds to the axial section in the central part of the specimen subjected to complex loading "proportional loading → tension". The results of the wavelet analysis provide an insight into the roughness

"frequencies". In Fig. 16(*b*), one can observe a significant increase in "frequencies" (by an order of magnitude) after deformation compared to the data for the reference configuration, which is associated with an increase in roughness due to the manifestation of the PLC effect and the formation of localized deformation bands on the specimen surface. The locations of bursts (protrusions on one-dimensional profile of the specimen surface), depending on the longitudinal coordinate, presumably correspond to the locations of localization of deformation bands that appear on the specimen surface during loading.

To form a prognosis of the deformation bands effect on the roughness of the specimen, it is advisable to compare the roughness profile along the loading axis with the dependence of radial deformations on the longitudinal (axial) coordinate. For this purpose, scalograms of the accumulated radial deformation values dependence on the coordinate at the moment of deformation completion and scalograms of one-dimensional surface profile in the central part of the axial section of the specimen under complex loading "proportional loading → tension" (14(*b*)) were plotted. The obtained data is shown in the form of scalograms in Fig. 18-19.

Roughness is determined by non-uniformity of radial deformations along the line on the surface parallel to the axial line. The case of small deformations is considered. In this case, due to the smallness of elastic deformations, the incompressibility condition can be adopted:

$$\varepsilon_r + \varepsilon_\theta + \varepsilon_Z \approx 0 \tag{4}$$

where ε_r are the components of radial deformation, ε_θ are the components of tangential (circumferential) deformation, ε_z are the components of axial (longitudinal) deformation.

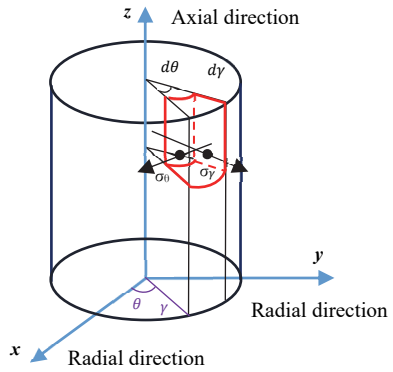

Figure 17: Axial direction and radial direction

The sector shown in Fig. 17 can be considered as a bar stretched in axial direction, the loading conditions of which in radial and circumferential directions are approximately the same. Then it can be assumed that the deformations $\varepsilon_r \approx \varepsilon_\theta$, and then from (4) we obtain $\varepsilon_r \approx -½\varepsilon_z$. The longitudinal deformation ε_z is measured directly in the experiment on complex loading. The graph of the calculated radial deformations from the axial coordinate is shown in Fig. 18(*a*).

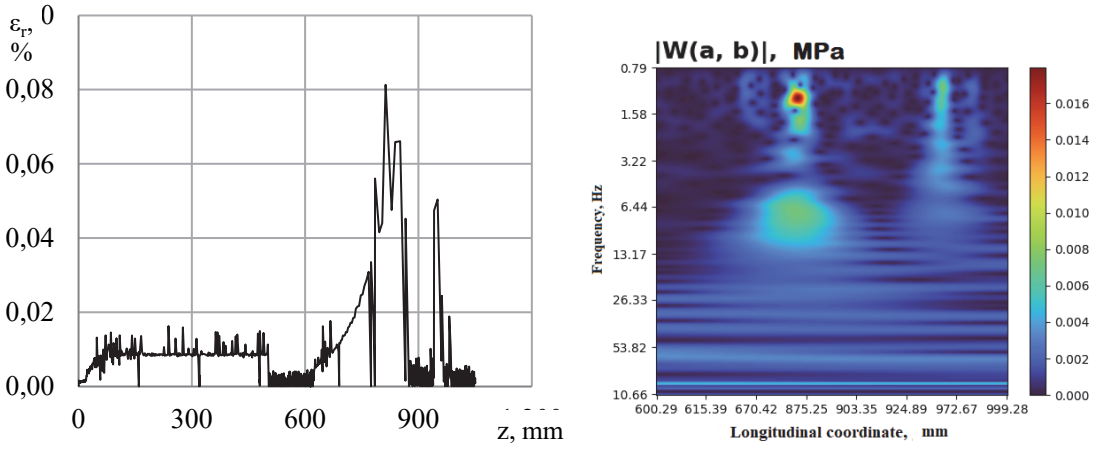

(*a*) (*b*)

Figure 18: Graph of the dependence of radial deformations of specimen No. 2 (*a*) and scalogram of the graph of radial deformations of specimen No. 2 (*b*).

To relate the location of the roughness obtained on the profilometer to the locations of the shear bands on the specimen, scalograms of the surface profile of specimen No. 2, shown in Fig. 14(*b*), and scalograms of the graph of radial deformations of specimen No. 2 were plotted; the results of the comparison of the scalograms are shown in Fig. 18 and 19. Fig. 18(*a*) shows the graph of radial deformations of specimen No. 2, and the scalogram of the graph of accumulated radial deformations is shown in Fig. 18(*b*).
The scalogram shown in Fig. 19(*b*) corresponds to one-dimensional surface profile in the central part of the axial section of a specimen under complex loading "proportional loading → tension".

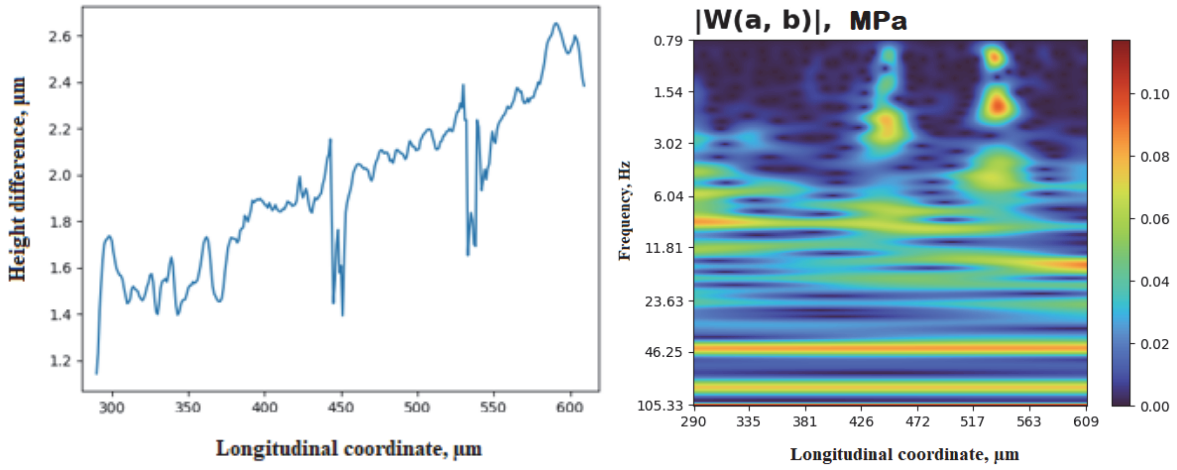

(*a*) (*b*)

Figure 19: Characteristic one-dimensional surface profile of specimen No. 2 after its deformation along the loading axis (*a*) and scalogram of the specimen surface profile after deformation (*b*).

The results of the wavelet analysis provide an insight into the roughness "frequencies". The scalogram of the dependence graph of specimen radial deformations and the scalogram of the specimen surface profile have a similar character. The characteristic bursts in the second half of the ranges in Fig. 18(*a*) and Fig. 19(*b*) arise due to the formation of deformation bands. Thus, the roughness leads to the formation of deformation bands on the specimen surface.

Conclusion

Ensuring high quality of products made of Al-Mg alloys due to their wide application is the most important task of organizing production at enterprises. The parameters used to assess the state of the surface layer are the geometric characteristics of the surface irregularities; which are assessed by the parameters of roughness, regular microreliefs, waviness [25].
The paper presents an analysis of the results of assessing the surface condition of thin-walled cylindrical specimens made of aluminum alloy after complex loading. Profilometric analysis of the deformation relief of the surface of aluminum alloy specimens after various programs of complex and simple loading made it possible to establish the presence of distinct patterns of sliding traces of deformation bands on the specimens' surface, which indicates the manifestation of the PLC effect under both simple and complex loading.
When loaded, the surface layer is deformed. In the initial period of loading, the roughness growth on the initially smooth surface is slow, but after the appearance of localized deformation bands, it increases. This can be explained by the increased brittleness of the damaged surface layer due to the accumulation of microdeformations. Dislocations come to the specimen surface, creating stress concentrators. Continuing loading causes the spread of deformation bands over the surface of the specimen and an increase in roughness.
A comparative analysis of the scale-invariant characteristics of Al-6%Mg alloy specimens in the initial state and deformed by complex loading allowed us to establish a significant increase in the Hurst exponent in a wide range of spatial scales, in contrast to undeformed specimens
The obtained results confirm that the manifestation of the PLC effect worsens the surface quality of finished metal products. At the same time, different loading programs worsen the surface quality to varying degrees (increase the surface roughness value). It can be concluded that uniaxial loading, to which specimens are subjected in most cases in experimental studies

[26, 27], is not sufficient for studying the properties of finished products and more diverse physical and mechanical tests are required, including complex loading, since complex loading programs used in the manufacture of various parts worsen the performance characteristics of products and can lead to sudden destruction.

ACKNOWLEDGES

The authors would like to express their sincere gratitude to P.V. Trusov for his help in preparing the article.
Mechanical tests were performed at the Center for Experimental Mechanics of Perm National Research Polytechnic University using the Unique Scientific Installation "Complex of testing and diagnostic equipment for studying the properties of structural and functional materials under complex thermomechanical effects".
The study was carried out with a financial support from the Ministry of Education and Science of the Russian Federation as part of the implementation of the national project "Science and Universities" (the state task fulfillment in the laboratory of multilevel structural and functional materials modeling, project no. FSNM-2024-0002).
The reported study was particularly supported by the Government Contract №124020200116-1 (experiments on interferometer profiler New View and fractal analysis conducted by Oborin V.A.).

REFERENCES

[1] Portevin, A. and Le Chatelier, F. (1923). Sur un phénomèneobservélors de l'essai de traction d'alliagesencours de transformation, Compt. Rend. Acad. Sci. Paris, 176, pp. 507-510.
[2] Bell, J.F. (1984). Mechanics of Solids: Volume I: The Experimental Foundations of Solid Mechanics, Springer Berlin Heidelberg, 825 p.
[3] McCormick, P.G. and Estrin, Y. (1989). Transient flow behaviour associated with dynamic strain ageing, Scripta Metallurgica, 23, pp. 1231-1234. DOI:10.1016/0036-9748(89)90332-3.
[4] Krishtal, M.M. (2004). Instability and mesoscopic inhomogeneity of plastic deformation (analytical review). Part II. Theoretical views on mechanisms of plastic deformation instability, Phys. Mesomech., 7 (5), pp. 5-29.
[5] Fridel, F. (1967). Dislocation. M.: Mir, 644 p.
[6] Cottrell, A.H. and Bilby, B.A. (1949). Dislocation theory of yielding and strain ageing of iron, Proc. Phys. Soc. A, 62 (1), pp. 49-62. DOI: 10.1088/0370-1298/62/1/308.
[7] Louat, N. (1981). On the theory of the Portevin – Le Chatelier effect, Scripta Metallurgica, 15 (11), pp. 1167-1170. DOI: 10.1016/0036-9748(81)90290-8.
[8] Yilmaz, A. (2011). The Portevin – Le Chatelier effect: a review of experimental findings, Sci. Technol. Adv. Mater., 12, 063001. DOI:10.1088/1468-6996/12/6/063001.
[9] Halim, H., Wilkinson, D.S. and Niewczas, M. (2007). The Portevin – Le Chatelier (PLC) effect and shear band formation in an AA5754 alloy, Acta Mater., 55, pp.4151-4160. DOI: 10.1016/j.actamat.2007.03.007.
[10] Benallal, A., Berstad, T., Børvik, T., Hopperstad, O.S. and Nogueira de Codes, R. (2008a). Effects of strain rate on the characteristics of PLC deformation bands for AA5083-H116 aluminium alloy, Philos. Mag., 88(28-29), pp. 3311-3338. DOI: 10.1080/14786430802468223.
[11] Li, X., Xu, Z., Guo, P., Peng, L. and Lai, X. (2022). Electroplasticity mechanism study based on dislocation behavior of Al6061 in tensile process, J. Alloys Compd, 910, 164890. DOI: 10.1016/j.jallcom.2022.164890.
[12] Lukáč, P., Balik, J. and Chmelik, F. (1997). Physical aspects of plastic instabilities, Mater. Sci. Eng. A.,234-236, pp.45-51. DOI: 10.1016/S0921-5093(97)00178-0.
[13] Casarotto, L., Dierke, H., Tutsch, R. and Neuhäuser, H. (2009). On nucleation and propagation of PLC bands in an Al–3Mg alloy, Mater. Sci. Eng. A., 527, pp.132-140. DOI: 10.1016/j.msea.2009.07.043
[14] Mehenni, M., Ait-Amokhtar, H. and Fressengeas, C. (2019). Spatiotemporal correlations in the Portevin-Le Chatelier band dynamics during the type B – type C transition, Mater. Sci. Eng. A., 756, pp.313-318. DOI: 10.1016/j.msea.2019.04.036.
[15] Chechulina, E.A., Oborin, V.A. and Gerasimov, R.M. (2024). Investigation of plastic flow localization by methods of structural analysis of surface relief morphology of aluminum alloy specimens, 31st Russian Conference on Mathematical Modelling in Natural Sciences, AIP Conf. Proc. 3183, 020005-1–020005-7. DOI: 10.1063/5.0225384.
[16] Tretyakova, T.V., Tretyakov, M.P. and Chechulina, E.A. (2021). Experimental study of the Portevin-Le Chatelier effect under complex loading of Al-Mg alloy: procedure issues, Frat. ed Integrità Strutt., 58, pp. 434-441.

DOI: 10.3221/IGF-ESIS.58.31.
[17] Trusov, P.V., Chechulina, E.A., Gerasimov, R.M., Vildeman, V.E. and Tretyakov, M.P. (2024). Using the wavelet transform to process data from experimental studies of the discontinuous plastic deformation effect, Frat. ed Integrità Strutt., 68, pp.159-174. DOI: 10.3221 / IGF-ESIS.68.10.
[18] Trusov, P.V., Wildemann, V.E., Chechulina, E.A., Tretyakova, T.V. and Tretyakov, M.P. (2022). Influence of a complex loading on a behavior of an aluminum alloy within the framework of the Portevin – Le Chatelier effect, Procedia Structural Integrity, 40, pp.433–439. DOI: 10.1016/j.prostr.2022.04.058.
[19] Zaiser, M. (2006). Scale invariance in plastic flow of crystalline solids, Adv. Phys., 55, pp. 185–245. DOI: 10.1080/00018730600583514.
[20] Bouchaud, E. (1997). Scaling properties of cracks, J. Phys. Condens. Matter., 9, pp. 4319– 4344. DOI: 10.1088/0953-8984/9/21/002.
[21] Feder, J., Danilov, Yu.A. and Shukurov, A. (1991). Fractals, M.: Mir, 254 p.
[22] Dyakonov, V.P. (2002). Wavelets. From theory to practice, M.: SOLON-R, 448 p.
[23] Novikov, L.V. (1999). Fundamentals of wavelet signal analysis: Textbook, St. Petersburg, IAnI RAS, 152 p.
[24] Goupillaud, P., Grossman, A. and Morlet, J. (1984). Cycle-octave and related transforms in seismic signal analysis, Geoexploration, 23 (1), pp. 85-102. DOI: 10.1016/0016-7142(84)90025-5.
[25] Stepanova, T.Yu. (2009). Technology of Surface Hardening of Machine Parts. A Textbook, Ivanovo: Ivanovsk. Gos. Univ. Khim. Tekhnol., 64 p. - ISBN – 5-9616-0315-4.
[26] Trusov, P.V. and Chechulina, E.A. (2014). Serrated yielding: physical mechanisms, experimental dates, macro-phenomenological models, PNRPU Mechanics Bulletin., 3, pp. 186-232. DOI: 10.15593/perm.mech/2014.3.10
[27] Trusov, P.V. and Chechulina, E.A. (2023). Methods and results of studying the Portevin – Le Chatelier effect: experiments and macrophenomenological models, PNRPU Mechanics Bulletin, 5, pp. 99-131. DOI: 10.15593/perm.mech/2023.5.09.